J. COMBIN. MATH. COMBIN. COMPUT. 127b (2025) 6219--6238

Journal of Combinatorial Mathematics and Combinatorial Computing
www.combinatorialpress.com/jcmcc

Combinatorial Press

Research on the optimization method of computational model in the design and application of subsurface fluid stratified sampling device

Anpin Zhou[1,✉], Shuyu Niu[2], Lei Zhang[3], Tan Liu[4], Hongwei Yin[5], Shi Wang[6], Jingze Song[7]

[1] *College of Disaster Prevention Engineering, Institute of Disaster Prevention, Shijiazhuang, Hebei, 050021, China*

[2] *School of Mathematics and Computer Science, Nanchang University, Shijiazhuang, Hebei, 050021, China*

[3] *School of Computer Science and Technology, Xidian University, Cangzhou, Hebei, 061000, China*

[4] *College of Disaster Prevention Technology, Department of Earthquake Science, Shijiazhuang, Hebei, 050021, China*

[5] *Earthquake Science Academy, Institute of Disaster Prevention, Shenzhou, Hebei, 053800, China*

[6] *Resource College, Hebei GEO University, Shijiazhuang, Hebei, 050021, China*

[7] *School of Information Science and Technology, Hebei Agricultural University, Shenzhou, Hebei, 053800, China*

ABSTRACT

In order to improve the automation and intelligence level of underground fluid sampling, this paper proposes a kind of underground fluid automatic sampling device, and carries out the structural design of the sampling device, the control system design and the field experiment test. According to the action process and movement characteristics of the underground fluid stratified sampling device, the control system needs to use multiple electromagnetic control valves to control the switching of the oil circuit of different actuators respectively. In order to improve the control state and response speed of the stratified sampling device system, a fuzzy identification algorithm is chosen to identify the control model, and the MIMO robust generalized predictive controller is used as the robust adaptive controller of the system to realize the low-flow and low-disturbance acquisition of underground fluids at the same monitoring point and at different depths. In the field sampling, the average values of DO at sampling depths of 1m, 2m, 3m, 4m, and 5m for manual sampling, vertical sampling, and fuzzy adaptive device sampling under the 1-2 sampling plumb line were 7.98mg/L, 7.86mg/L, 8.25mg/L, 7.83mg/L, and 7.77mg/L, respectively. The deviation of dissolved oxygen content at the same sampling point in the three ways is small and the trend of change is consistent at different depths. It shows that the fuzzy adaptive stratified sampling device system designed in this paper can be applied to the sampling of subsurface fluids with dissolved oxygen as the detection target.

Keywords: fuzzy identification algorithm, MIMO, fuzzy adaptive, stratified sampling

✉ Corresponding author.
E-mail address: 15930119247@163.com (A. Zhou).

Received 01 March 2024; Revised 25 May 2024; Accepted 10 November 2024; Published Online 16 April 2025.
DOI: 10.61091/jcmcc127b-341

1. Introduction

The sustainable development of energy, resources and environment is a major issue concerning the future development of mankind, and the technological development in this field reflects the core competitiveness of the country and the living standard of the people [1]. However, in the process of requesting energy, resources and strategic space from the underground, with the increasing demand for underground resources, the irrational exploitation and utilization of underground resources have led to the continuous decline of the groundwater level, accompanied by the change, pollution, destruction and even threat to human health of the environment of the underground, the surface and the air [2-5]. For example, the problem of groundwater over-exploitation is becoming more and more prominent, and the extreme imbalance between the amount of groundwater extraction and the amount of recharge makes the groundwater level continue to decline, forming a large over-exploitation area and a groundwater landing funnel, which has caused a serious impact on the sustainable cycle of water resources and the balance of the ecological environment. At present, about 2/3 of the global area is facing the problem of water resources shortage, which has a serious impact on people's production and life [6]. China is also a water-scarce country, and it has been reported that there are 164 groundwater over-mining areas in China, totaling 181,300 km2, of which 77,000 km2 are severely over-mined [7]. Over-exploitation of groundwater not only causes the local groundwater level to fall, changes the natural flow field of the groundwater system, which in turn affects the quality of groundwater, and triggers a series of negative environmental and ecological effects, such as ground subsidence, subsidence, cracks, seawater intrusion, and continuous deterioration of the ecological environment [8-11]. Therefore, it is of great practical significance for China's ecological environmental protection and sustainable economic development to grasp the situation of groundwater exploitation and utilization in a timely manner.

Meanwhile, groundwater in China is generally threatened by pollution caused by urbanization, industrialization, agriculture and mining activities. Ninety percent of urban groundwater in China is contaminated by organic and inorganic toxic and hazardous substances such as nitrates and aromatic hydrocarbons, and the contamination has been expanding from point to point, from shallow to deep, and from urban to rural areas, and the degree of contamination is becoming more and more serious. Groundwater contamination is not easy to detect in the early stage, and it is covert and delayed [12-15]. Anthropogenic pollutants diffuse into the groundwater, because of its relatively slow migration rate and deep underground, if not long-term special monitoring, it is difficult to find groundwater pollution, and found when the groundwater has been contaminated or seriously contaminated [16-17]. In addition, the groundwater system has a unified hydraulic connection and spatio-temporal succession law, in constant transport and circulation, experiencing recharge, runoff, discharge pathways [18]. In the complex system of geo-environment, each hydraulic system has close hydraulic connection, that is, when groundwater pollution occurs, the scope of pollution is difficult to circle and difficult to restore. Therefore, continuous monitoring and analysis of the underground environment is an important measure for the prevention of groundwater pollution, which can be used as a direct evidence for determining the degree of environmental pollution and responsibility attribution of the project or enterprise [19-20]. Based on this, the development of subsurface fluid sampling technology is increasingly important.

Subsurface fluid sampling combined with isotope tracking, stratigraphic residual gas analysis, chemical composition testing and other means can provide a large amount of stratigraphic information, which is one of the important means to carry out the evaluation of groundwater resources and environmental monitoring, and is of guiding significance for the safe conduct of engineering and environmental risk assessment, and there is a large number of engineering needs [21-23]. Subsurface fluid sampling technology plays an important role in subsurface pollution prevention and control, subsurface environmental monitoring and subsurface chemical characterization, the accuracy and precision of subsurface test results depend largely on the quality of the subsurface samples obtained, and whether or not in-situ subsurface samples can be collected in the target section is the key to the success of subsurface monitoring and control and whether or not subsurface circulation analysis is correct [24-27]. Since the existing subsurface fluid sampling techniques cannot satisfy the increasing demands of groundwater resources evaluation and environmental monitoring, and some of the sampling techniques are far away from the international first-class level, it is urgent to research and develop the fluid sampling techniques and equipments with high technological content and independent intellectual property rights for the subsurface environment.

This paper analyzes the structure and working principle of the automatic sampling device, and preliminarily designs the overall scheme of the underground fluid stratified sampler. The working process of the sampling device is analyzed, and the complete action flow of single underground fluid sampling is refined. By fuzzy theory and MIMO nonlinear system, the control system of stratified sampling device is recognized. Adjust the design of the identification method to decompose the auxiliary control system with three inputs and three outputs into three systems with three inputs and one output, which become the temperature part, the acidity and alkalinity part, and the flow rate part, respectively. A robust adaptive controller is added to the stratified sampling device system for the adaptive control process of the subsurface fluid stratified sampling auxiliary device. Simulation tests as well as field subsurface fluid sampling are carried out to analyze and verify the reliability of the stratified sampling device system supported by the fuzzy identification algorithm.

2. Design of stratified sampling devices

2.1. *Structure and working principle of the automatic sampling device*

Automatic sampling devices are specialized for fluids and consist of three parts: detector, controller and actuator [28-30]. Among them, the detector is divided into time detection and flow detection, the controller is a solenoid valve, and the actuator is an electronically controlled pneumatic ball valve. When the detector detects the time or flow rate, it transmits the detection signal to the controller, which controls the opening and closing of the pneumatic ball valve and the duration of opening. The ball valve starts sampling from the closed state to the open state, and ends sampling from the open state to the closed state. The controller controls the time from opening to closing of the ball valve to control the amount of sampling.

2.2. *Overall program for stratified samplers of subsurface fluids*

The sampler is used to realize low-flow, low-disturbance collection of underground fluids at different depths at the same monitoring point. It monitors the effect of layered groundwater containment, excludes the influence of well-hole stagnant water, and makes the collected water samples representative. In the collection process, in order to obtain underground fluids at different levels, self-expanding packer is utilized to separate them, and screw pumps are selected for stratified extraction. In order to realize low-flow and low-disturbance sampling, the screw pump is used in conjunction with a frequency converter. The overall scheme of the underground fluid stratified sampler is shown in Figure 1.

The monitoring platform is analyzed by big data and communicates with the host computer through the Internet of Things. The sampler controls the inverter and frequency adjustment based on the instructions from the host computer to realize sampling of different flow rates. Through the water level monitoring probe to determine the downhole water level changes and the sealing effect of the self-expanding rubber packer. Multi-parameter sensors integrating temperature, pressure and conductivity are placed in the flow cell to eliminate the influence of stagnant water in the groundwater wells and obtain fresh groundwater. Through the true value determination, it realizes many functions such as power supply on and off of the sampling system, automatic collection and determination of water sample parameters, controlling the feeding and discharging of water samples, processing of terminal commands, and on-line transmission of data.

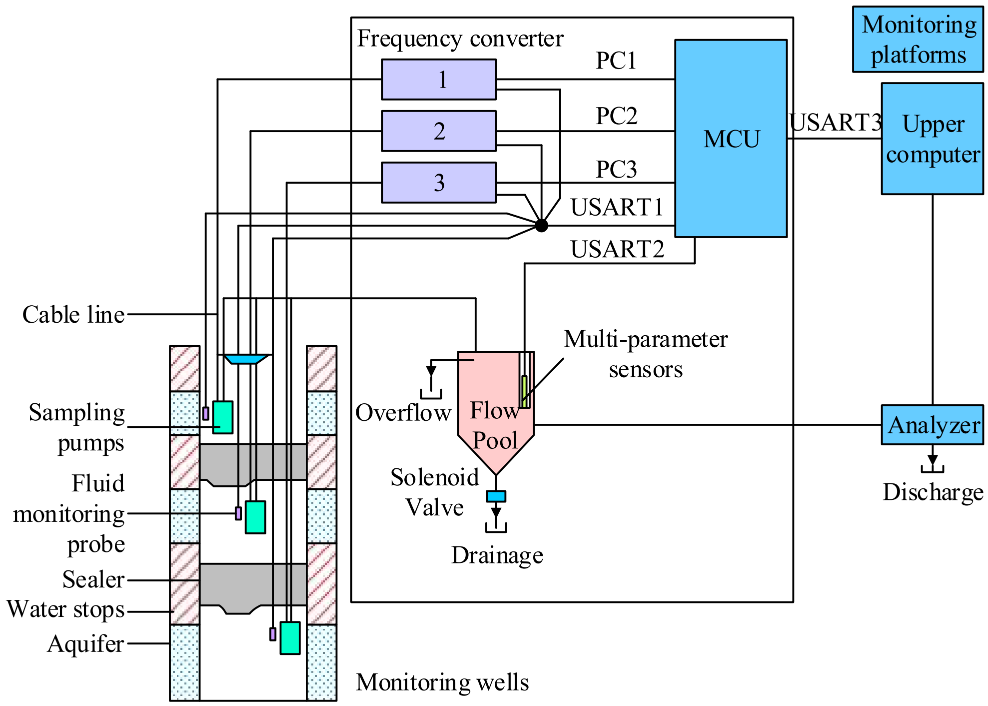

Fig. 1. The overall solution of the underground fluid layer sampler

2.3. Sampling action timing analysis

Through the analysis of the stratified sampling device, the sampling process is realized through a series of hydraulic cylinders and hydraulic vibration hammer successive matching action. Hydraulic cylinders and hydraulic vibration hammer switch and direction of action is controlled by electromagnetic reversing valve. Electromagnetic reversing valve is directly manipulated by the electromagnet to switch the direction of the control valve, is an important control element in this paper underground fluid sampling control system, used to control the actuator start, stop and direction control. According to the action process and movement characteristics of the underground fluid stratified sampling device, the control system needs to use five electromagnetic control valves to control the switching of the oil circuit of five actuators.

Electromagnetic control valve configuration is as follows:

1) Support cylinder: choose three four-way double-acting solenoid valve control, neutral function for O, oil pressure is not unloaded, control the position of the guided support frame, solenoid named DT11, DT12.

2) Lifting cylinder: three four-way double-acting solenoid valve control, the center position can be O, the hydraulic pressure is not unloaded, can make the hydraulic impactor slide seat in the guiding support frame at any position to stop, solenoid named DT21, DT22.

3) Outrigger cylinder: three four-way double-acting solenoid valve control, the center position can be O, oil pressure is not unloaded, can make the outrigger disk in any position to stop, solenoid named DT31, DT32.

4) Hydraulic vibratory hammer circuit: two-position two-way single-acting solenoid control valve is used, its role is equivalent to an oil switch. The solenoid is named DT4.

5) Unloading circuit: adopting two-position two-way single-acting electromagnetic control valve, whose function is equivalent to an oil switch. The solenoid is named DT5.

The travel switches are configured as follows:

(1) KT11: Judge the initial position of the support cylinder, the initial state is closed.

(2) KT12: Judge whether the support cylinder reaches the position required for sampling work, the initial state is closed.

(3) KT21: Judge the initial position of the outrigger cylinder, the initial state is closed.

(4) KT22: Judge whether the outrigger cylinder reaches the position required for sampling work, the initial state is disconnected.

(5) KT31: Judge the initial position of the lifting cylinder, the initial state is closed.

(6) KT32: Judge whether the lifting cylinder is at the lowest point in the sampling process, the initial state is disconnected.

(7) KT33: Judge whether the lifting cylinder reaches the predetermined height to open the hydraulic hammer, the initial state is disconnected.

The complete action flow of single underground fluid sampling is as follows: the support cylinder acts firstly to make the guiding support frame slowly erected until it is perpendicular to the ground. The outrigger cylinder starts to act, lowering the universal outrigger disk so that it is in close contact with the ground surface, forming a stable support point to prevent the sampling vehicle from tipping over due to the unstable center of gravity during the sampling process. The lifting cylinder rises, and the driving slide drives the hydraulic impact hammer to move up to the highest point along the guide support frame rail, and installs the soil sampling pipe at the lower end of the impactor. After installation, the lifting cylinder descends, and at the same time opens the hydraulic vibration hammer, repeatedly vibrating the underground fluid sampling tube, sampling operations. When the sampling tube reaches the required sampling depth, the hydraulic vibration hammer stops moving, the lifting cylinder rises back to the predetermined position, removes the sampling tube, and obtains the underground fluid sample. After the sampling is completed, the outrigger cylinder and support cylinder recover the outrigger disk and guide support frame to the initial position.

3. Adaptive control of automatic sampling devices

3.1. Fuzzy adaptive control

The basic structure of fuzzy control system consists of fuzzy controller, actuator, controlled object and sensor. Among them, the structure of the fuzzy controller is the core part of the composition of the fuzzy control system [31].

According to the number of input variables of the fuzzy controller, the fuzzy controller can be categorized into univariate fuzzy controller and multivariate fuzzy controller, in which the univariate fuzzy controller has more applications. The number of input variables of a univariate fuzzy controller is defined as the dimension of the fuzzy control.

The fuzzy inference algorithm of Mamdani fuzzy model uses the minimal operation rule to define the fuzzy relations expressed by the fuzzy implication and the rule is as follows:

$$R: \textit{If } x \textit{ is } A \textit{ then } y \textit{ is } B \tag{1}$$

where x is the input linguistic variable, A is the fuzzy set of inference antecedents. y is the output linguistic variable, and B is the posterior of the fuzzy rule. The fuzzy relation is denoted by Rc:

$$Rc = A \times B = \int_{x \times y} \mu_A(x) \wedge \mu_B(y) f(x, y) \tag{2}$$

When x is A' and the fuzzy relationship is synthesized using the “very large - very small” operation, the conclusion of the fuzzy inference is calculated as follows:

$$B' = A' \cdot Rc = \int_y \bigvee_{x \in X} \left(\mu_A(x) \left(\mu_A(x) \wedge \mu_B(x) \right) \right) / y \tag{3}$$

The output obtained after inference of each rule of the Mamdani model is a distributional affiliation function or discrete fuzzy set of variables. After synthesizing the results of multiple rules, the fuzzy sets of each output variable need to be defuzzified to obtain the actual desired output. Usually, there are four main methods for defuzzification: maximum affiliation function method, median method, center of gravity method and weighted average method.

MIMO nonlinear system [32]:

$$\begin{gathered} y_1^{(r)} = f_1(x) + \sum_{j=1}^{p} g_{1j}(x) u_j \\ \vdots \\ y_p^{(r_p)} = f_p(x) + \sum_{j=1}^{p} g_{ij}(x) u_j \end{gathered} \tag{4}$$

where state quantity $x = \left[y_1, \dot{y}_1, \cdots, y_1^{(r_1 - 1)}, \cdots, y_p, \cdots, y_p^{(r-1)} \right]^T$ is measurable. $u = \left[u_1, \cdots, u_p \right]^T$ is an input variable, $y = \left[y_1, \cdots, y_p \right]^T$ is an output variable. $f_i(x)$, $g_{ij}(x)$ are smooth unknown nonlinear functions, and $i, j = 1, 2, \cdots, p$.

Let:

$$y^{(r)} = \left[y_1^{(f_1)}, \ldots, y_p^{(r_p)} \right]^T \tag{5}$$

$$F(x) = \left[f_1(x), \cdots, f_p(x) \right]^T \tag{6}$$

$$G(x) \begin{bmatrix} g_{11}(x) & \cdots & g_{1p}(x) \\ \vdots & \ddots & \vdots \\ g_{p1}(x) & \cdots & g_{pp}(x) \end{bmatrix} \tag{7}$$

Then equation (4) can be expressed as:

$$y^f = F(x) + G(x) u \tag{8}$$

By designing the control law $u(t)$, it can be ensured that all variables of the closed-loop system are bounded and it is the output of the system that tracks a given desired trajectory $y_d(t) = \left[y_{d1}(t), \cdots, y_{dp}(t) \right]^T$.

Assumption 1: $G(x)$ is a positive definite matrix and there exists a real number $\delta_0 > 0$ that satisfies $G(x) \geq \delta_0 I_P$.

Assumption 2: The desired trajectories $y_{di}(t)$, $i = 1, \cdots, p$, are bounded and there exist r_ith order derivatives and all order derivatives are bounded.

Define the trajectory tracking error as:

$$\begin{gathered} e_1(t) = y_{d1}(t) - y_1(t) \\ \vdots \\ e_p(t) = y_{dp}(t) - y_p(t) \end{gathered} \tag{9}$$

Define the filter tracking error function:

$$
\begin{gathered}
s_1(t) = \left(\frac{d}{dt} + \lambda_1\right)^{r_1 - 1} e_1(t)\lambda_1 > 0 \\
\vdots \\
s_p(t) = \left(\frac{d}{dt} + \lambda_p\right)^{t_t - 1} e_p(t)\lambda_p > 0
\end{gathered}
\tag{10}
$$

From equation (10), when $s_i \to 0$, $e_i \to 0(i = 0,1,2,\cdots,p)$, then the control objective can be transformed to $s_i \to 0(i = 1,2,\cdots,p)$.

This can be obtained according to Newton's binomial theorem:

$$
\begin{gathered}
\dot{s}_1 = v_1 - f_1(x) - \sum_{j=1}^{p} g_{1j}(x)u_j \\
\vdots \\
\dot{s}_p = v_p - f_p(x) - \sum_{j=1}^{p} g_{pj}(x)u_j
\end{gathered}
\tag{11}
$$

Let $s(t) = \left[s_1(t)\cdots s_p(t)\right]^T$, $v(t) = \left[v_1(t)\cdots v_p(t)\right]^T$, then equation (11) can be expressed as:

$$
\dot{s} = v - F(x) - G(x)u \tag{12}
$$

The nonlinear functions $F(x)$ and $G(x)$ are known, then the following linear control law can be used:

$$
u = G^{-1}(x)\left(-F(x) + v + K_0 s\right) \tag{13}
$$

where $K_0 = diag\left[k_{01},\cdots,k_{op}\right]$, $k_{0t} > 0$, and $i = 1,\cdots,p$.

Therefore, when $f_i(x)$ and $g_{ij}(x)$ are known, the control law Eq. (13) is easily obtained. However, in the actual system, the nonlinear functions $f_i(x)$ and $g_{ij}(x)$ are unknown and it is not possible to design the control law Eq. (13), and a fuzzy system can be used to approximate the nonlinear functions $f_i(x)$ and $g_{ij}(x)$.

3.2. *Sampling device fuzzy modeling*

A fuzzy identification algorithm is utilized to identify the control system of a stratified sampling device so that a suitable fuzzy modeling mechanism can be selected. The sampling device of the auxiliary system of the biological underground fluid monitoring system is a multivariate controlled object with certain interactions. The structure of the sampling system control object is shown in Fig. 2. In the figure, U_Q, U_D and U_W represent the switching frequency command of the quick heating device, the speed command of the peristaltic pump for dechlorination solution and the speed command of the pump for experimental water samples, and P_H, T_E and F_L represent the acidity and alkalinity of the water samples, the temperature of the water samples and the flow rate of the water samples, respectively.

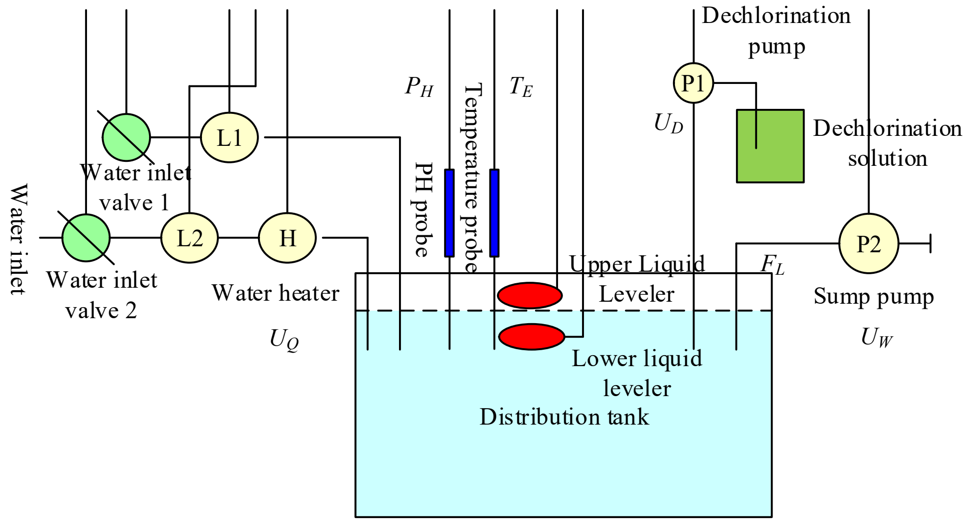

Fig. 2. The sampling system controls the object structure

The input as well as output relationship of an object can be represented by the following equation:

$$\begin{bmatrix} T_E \\ P_H \\ F_L \end{bmatrix} = \begin{bmatrix} W_{TQ} & W_{\mathrm{D}} & W_{TW} \\ W_{PQ} & W_{PD} & W_{PW} \\ W_{FQ} & W_{FD} & W_{FW} \end{bmatrix} \cdot \begin{bmatrix} U_Q \\ U_D \\ U_W \end{bmatrix} \tag{14}$$

where W_{TQ}, W_{PQ} and W_{FQ} are the transfer functions with U_Q as input, T_E, P_H and F_L as output, respectively (U_D and U_W are held constant). W_{TD}, W_{PD} and W_{FD} are transfer functions with U_D as input, T_E, P_H and F_L as output respectively (U_Q and U_W remain unchanged). W_{TW}, W_{PW} and W_{FW} are transfer functions with U_W as input, T_E, P_H and F_L as output respectively (U_Q and U_D remain unchanged).

The dynamic characteristics of the controlled object used in the design process are shown in the following set of equations:

$$\begin{cases} W_{TQ}(s) = \dfrac{4.32s}{(1+6s)(1+9s)} \\ W_{PQ}(s) = \dfrac{11.26s}{(1+20s)(1+37s)} \\ W_{FQ}(s) = \dfrac{1.54s}{(1+3s)(1+11s)} \end{cases} \tag{15}$$

$$\begin{cases} W_{TD}(s) = \dfrac{30.258s}{(1+2s)(1+13s)} \\ W_{PD}(s) = \dfrac{11.17s}{(1+65s)(1+124s)} \\ W_{FD}(s) = \dfrac{1.54s}{(1+71s)(1+86s)} \end{cases} \tag{16}$$

$$\begin{cases} W_{TV}(s) = \dfrac{3.62s}{(1+31s)^2} \\ W_{PW}(s) = \dfrac{1.26s}{(1+39s)^2} \\ W_{FW}(s) = \dfrac{4.03s}{(1+33s)^2} \end{cases} \tag{17}$$

In order to test the performance of the recognition method in the case of large and frequent changes in the input of the controlled object, U_Q, U_D and U_W are taken as uncorrelated pseudo-random sequences. The step size of signals U_Q, U_D and U_W is taken to be 8s, and the amplitude of change is 3% of the design value. The number of steps in each cycle of signal U_Q is set to be 20, that of signal U_D to be 31, and that of signal U_w to be 68.

According to the needs of the identification method, the three-input, three-output auxiliary control system is decomposed into three three-input, single-output systems, which become the temperature part, the pH part and the flow rate part, respectively.

The dynamic response speed of each channel of the hierarchical sampling control system varies greatly, e.g., the dynamic response of $U_Q \to T_E$ is much faster than that of $U_D \to T_E$. Therefore, how the generalized input variables of the fuzzy model are selected becomes a key element affecting the quality of identification and control.

Take the dynamic characteristic identification of a three-input-single-output sampling object as an example to illustrate the prerequisites of the fast identification model. First of all, the simplified mathematical model of the controlled object should be obtained, and the simplified model of the water sample temperature of the stratified sampling device is shown in equation (18):

$$T_\varepsilon(t) = \frac{1.15}{(1+6.37s)} u_Q(t) + \frac{0.87}{(1+2.43s)} u_D(t) + \frac{4.32}{(1+5.29s)} u_W(t) \tag{18}$$

Where s is the Laplace transform factor, $T_E(t)$ is the water sample temperature index of the sampling aid, $u_Q(t)$ is the opening degree of the quick heating device, (1%), $u_D(t)$ is the opening degree of the pumping device (1%), $u_W(t)$ is the opening degree of the dechlorination device (1%). Take $u_Q(t)$, $u_D(t)$ and $u_w(t)$ as uncorrelated pseudo-random sequences with a step size of 40s and a variation amplitude of $\pm 30\%$. $u_Q(t)$ The number of steps in the signal cycle is 15, $u_D(t)$ is 31, and $u_w(t)$ is 63. Take the sampling period as 2s and the data logging period as 40s.

The performance index is taken as:

$$PER = \left[\frac{1}{50} \sum_{k=1}^{50} \left(T_E(t) - \hat{T}_E(t) \right)^2 \right]^{1/2} \tag{19}$$

Eq. $\hat{T}_E(t)$ represents the output value of the k nd sampling moment calculated by the fuzzy model of mountain identification.

Extension to three three-input-single-output sampling objects for dynamic identification. The controlled objects of the auxiliary system have three inputs and three outputs. For the three-input-single-output control system, the ordinary CARIMA model can be obtained. After integration, the CARIMA dynamic model of the three-input and three-output auxiliary system can be obtained. After obtaining the CARIMA model, its controller can be designed.

3.3. Design of robust adaptive controller in sampling device

The fuzzy model identification method of hierarchical sampling device model can solve the problem of uncertainty and nonlinearity of the control system with high model accuracy. Compared with the common fuzzy identification method, multiple linear regression is used to identify the conclusion structure and conclusion parameters, which reduces the computation amount and improves the convergence and identification speed.

1) The design of the robust controller of the stratified sampling device is as follows:

The structure of the robust adaptive controller for the stratified sampling system is shown in Fig. 3. Where $G_p\left(z^{-1}\right)$ represents the transfer function matrix of the controlled object of the sampling device, which is transformed out of the discriminative fuzzy model. It can be expressed as:

$$G_p\left(z^{-1}\right)=A^{-1}\left(z^{-1}\right)B\left(z^{-1}\right) \tag{20}$$

Here the coefficients of each of $A^{-1}\left(z^{-1}\right)$ and $B\left(z^{-1}\right)$ are time-varying parameter matrices, which are dynamically determined online by fuzzy identification method. $D(t)$ refers to the system perturbation input vector, including water sample pH perturbation, water sample temperature perturbation and water sample flow rate perturbation.

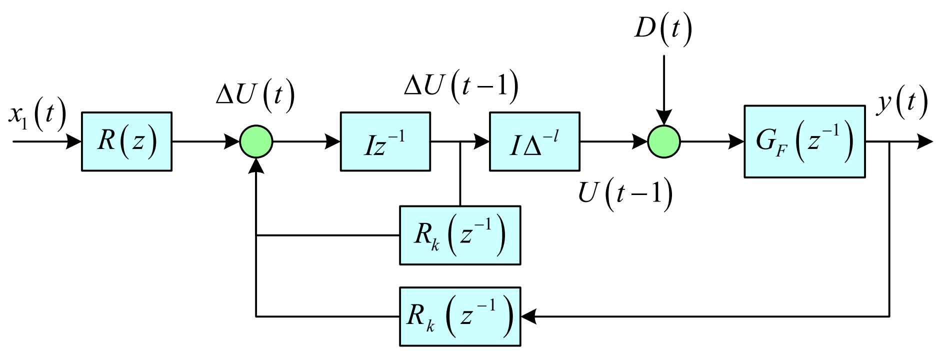

Fig. 3. The hierarchical sampling system is robust adaptive controller structure

2) Stability Evaluation of Robust Adaptive Controller in Stratified Sampling Device. From the above figure the open loop transfer function matrix of the system is given as:

$$Q_0\left(z^{-1}\right)=A^{-1}\left(z^{-1}\right)B\left(z^{-1}\right)\left(Iz+R_u\left(z^{-1}\right)\right)^{-1}\Delta^{-1}R_y\left(z^{-1}\right) \tag{21}$$

The closed-loop stability of this controller is judged according to the following criteria:

(1) The closed-loop system is stable when and only when the sum of the number of times the characteristic trajectory of $Q_0\left(e^{-j\omega T}\right)$ (ω is the angular frequency and T is the sampling period) contains $(-1, j_0)$ points counterclockwise equals the number of unstable poles of the open-loop system.

(2) The closed-loop system is stable when and only when all closed-loop poles of the MIMO system fall within the unit circle, and the closed-loop system poles can be calculated by the following characteristic equation:

$$\det\left[I+Q_0\left(z^{-1}\right)\right]=0 \tag{22}$$

The above two guidelines provide a theoretical basis for the analysis of MIMO fuzzy adaptive control systems. For the unstable and non-minimum-phase auxiliary system sampling device control object, when the design parameter $\left(N, N_u, P(j), Q(j)\right)$ of the adaptive controller is appropriately chosen so that the matrix polynomials $R_u\left(z^{-1}\right)$ and $R_y\left(z^{-1}\right)$ are tuned, all the zeros of the closed-loop characteristic equations can be made to fall within the unit circle. Thus, this robust generalized predictive controller can be used to control the auxiliary system sampling device and is capable of overcoming system instabilities and external disturbances.

4. Sampling device model optimization and application

4.1. Simulation analysis of the optimization model of the sampling device

The control performance of the nonlinear adaptive controller is shown in Fig. 4. y(k) produces large fluctuations at the beginning of the operation of the sampling device system. When k is greater than or equal to 25, y(k) always fluctuates around $y_r(k)$ to produce a small range of fluctuations, the interference signal is small, and the system always maintains a stable state. The white noise of the optimized sampling device system is controlled within the range of [-1,1]. The system performance obtained by the improvement method proposed in this paper is excellent, with most moments of the switching sequence selecting the control inputs of the demand-designed nonlinear adaptive controller. However, when the nonlinear model does not perform well due to special factors, the switching method temporarily selects the line adaptive controller to generate the system inputs, and then chooses to continue the switching when the nonlinear model's discriminative effect occurs the next time, and the system has upper and lower bounds for any signals in the switching adaptive control system, and it has excellent control states and transient response modes.

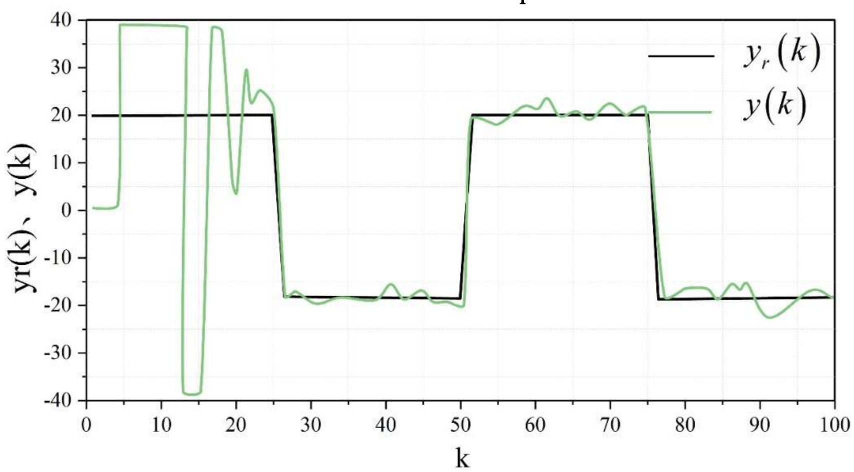

(a) $y_r(k)$、$y(k)$

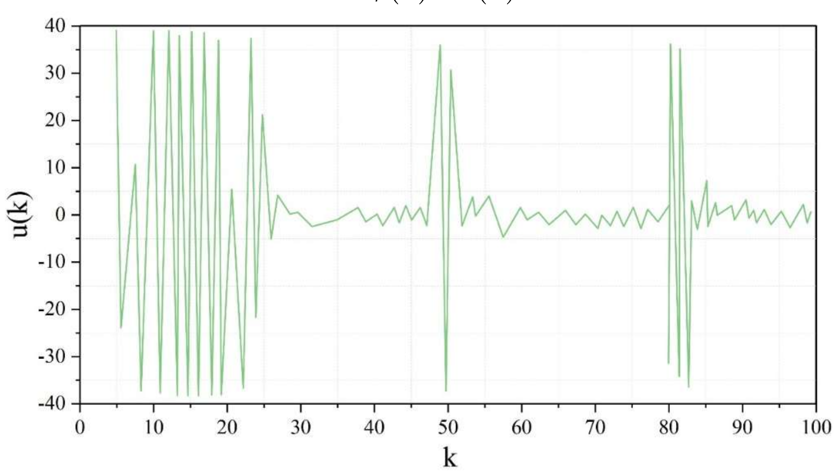

(b) u(k)

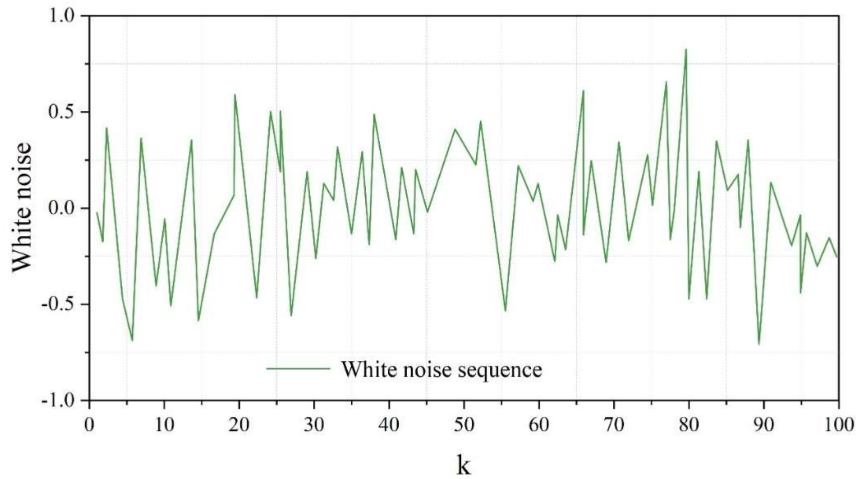

(c) White noise sequence

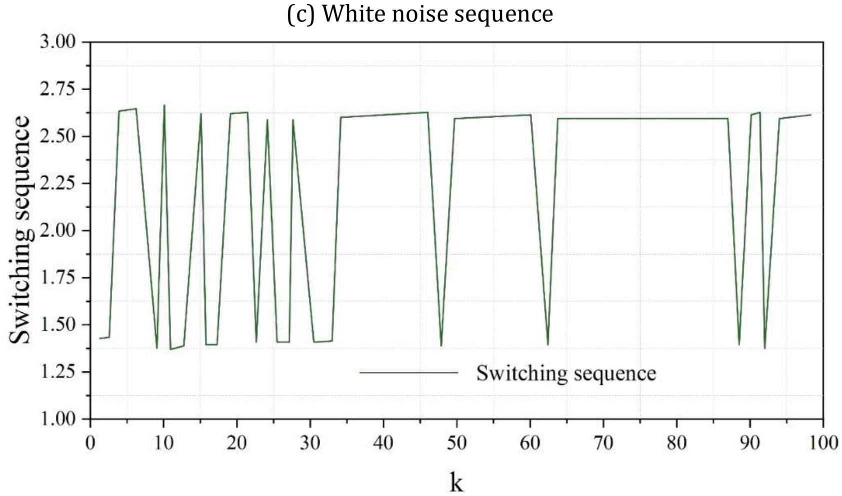

(d) Switching sequence

Fig. 4. Control power of nonlinear adaptive controller

4.2. Performance tests of automatic subsurface fluid sampling devices

The structure design and control system design of the automatic underground fluid sampling device were completed in the previous section. After the design was completed, this chapter tested the performance of the prototype, and designed different depth sampling tests in non-automatic control mode and fixed depth sampling tests in automatic control mode, respectively, and evaluated the performance of the whole machine with the evaluation indexes of sampling time, fluid weight, and navigation tracking accuracy.

In order to verify the stability and reliability of the prototype in executing the automatic sampling process, the automatic sampling performance test was conducted in January 2025 at a test site.

Before the start of the test, the subsurface fluid sampling device was mounted on a tracked chassis, and the chassis was moved to any point within the test site by remote control, and 18 sampling points were randomly selected near the point for the automatic sampling test. The results were analyzed using the sampling time error and the weight of the underground fluid as evaluation indexes.

Three different sampling depths of 10cm, 20cm and 30cm were set up in the test, and six samples were collected at each depth, each sample was kept in a transparent self-sealing bag with a self-weight of 3g. At the same time, the operation of the sampling mechanism, fluid mechanism and collection mechanism was observed to check whether the subsurface fluid would adhere to the sampling rod when ejecting and whether it could completely fall into the sub-cassette of the collection mechanism. During sampling, the push rod and rotary motor moved at a constant speed, and the lift speed of the push rod was set at 15mm/s, and the rotary speed at 60r/min.

The sampling depth is adjusted by setting the detection critical value of the ultrasonic distance sensor in the control system software. When the sampling depth is 10cm, 20cm and 30cm, the ultrasonic detection distance critical value is set to 20cm, 10cm and 5cm in turn, and the corresponding theoretical sampling time is 92s, 100s and 110s respectively. Each time a sample is taken, the software automatically records the length of the sample, and comparing the actual sampling time with the theoretical sampling time allows the stability of the automatic sampling process to be analyzed. After 18 samples were collected, each sample was weighed, and further, the mean and standard deviation were calculated for the net weight of six samples of the same depth.

Information on the samples collected from the 18 sampling points in the experiment is shown in Table 1, from top to bottom, six samples of subsurface fluids at depths of 10 cm, 20 cm and 30 cm. Calculate the sampling time error, weight and net weight for each sample as well as the mean, standard deviation of the weight for samples from the same depth.

From the test results, it can be seen that the sampling time length is proportional to the sampling depth, and the sampling time length errors are all zero, which satisfies the theoretical time length calculation formula. The sampling time length of the same depth is the same, which indicates that the system can operate stably during sampling and can realize the sampling depth adjustment. When the sampling reached the deepest depth of 30cm, the sampling time was the longest 110 s. The weight of the samples also increased with the increase of the sampling depth. The difference between the sample weights at 10cm depth was small, with a maximum value of 7.38 g and a minimum value of 6.25 g. The difference between the sample weights at 20cm depth was large, with a maximum value of 16.58 g and a minimum value of 11.67 g. The standard deviation increased with the deepening of the sampling depth, which indicated that the deeper the sampling depth, the greater the fluctuation of the sample weights.

Table 1. Sample information collected at 18 sampling points in the experiment

Sampling Depth /(cm)	N	(x,y)/(m)	Sample weight /(g)	Mean net weight/(g)	Average/ (g)	SD /(g)	Max /(g)	Min /(g)
10	1	(-257.143,-214.474)	8.46	6.25	6.76	0.517	7.38	6.25
	2	(-254.065,-204.623)	9.23	7.38				
	3	(-251.127,-221.196)	9.54	6.93				
	4	(-255.009,-211.566)	8.96	6.07				
	5	(-253.425,-215.004)	9.15	6.78				
	6	(-252.235,-219.163)	9.87	7.17				
20	1	(-257.558,-215.142)	10.54	8.59	9.54	0.922	10.52	8.59
	2	(-254.127,-206.254)	13.09	10.12				
	3	(-251.526,-221.173)	12.84	10.52				
	4	(-255.234,-211.554)	11.37	9.73				
	5	(-253.215,-215.212)	10.55	8.78				
	6	(-252.669,-219.309)	12.01	9.51				
30	1	(-257.082,-215.542)	16.54	13.54	13.95	1.52	16.58	11.67
	2	(-254.916,-206.354)	14.99	11.67				
	3	(-251.604,-221.549)	15.25	13.06				
	4	(-255.512,-215.186)	18.83	16.58				
	5	(-253.774,-213.054)	15.64	13.82				
	6	(-252.321,-218.289)	17.78	15.03				

During the test, it was found that each mechanism of the sampling device operated smoothly and could complete the underground fluid collection process according to the settings of the control program.

The changes of sampling time, average and standard deviation of fluid weight with sampling depth are shown in Fig. 5, and the average weights of underground fluids obtained at sampling depths of 10cm, 20cm and 30cm were 6.76g, 9.54g and 13.95g respectively.

Each time the collection of subsurface fluid was performed, the top bar was able to eject the fluid from the pickup rod, and no fluid adhesion to the top bar and pickup tube occurred. The collection device was rotated to directly underneath for collection, and the collection inner box was automatically reset when six samples were completed. The sampling time for each sample was accurate and the system operated stably. Due to the influence of the topography of different sampling points, the weight of different underground fluids at the same depth varies slightly, with the shallow layer having a lower content, and the collected samples are looser and lighter in weight. With the deepening of the depth, the underground fluid content increases and the weight of the removed fluid is larger. The sampling device performs stably in the sampling process, the fluid weight fluctuation range is small, and it can collect underground fluids in the depth range of 0~30cm in layers, and complete the underground fluid collection in a short period of time, the system runs stably and the sampling efficiency is high.

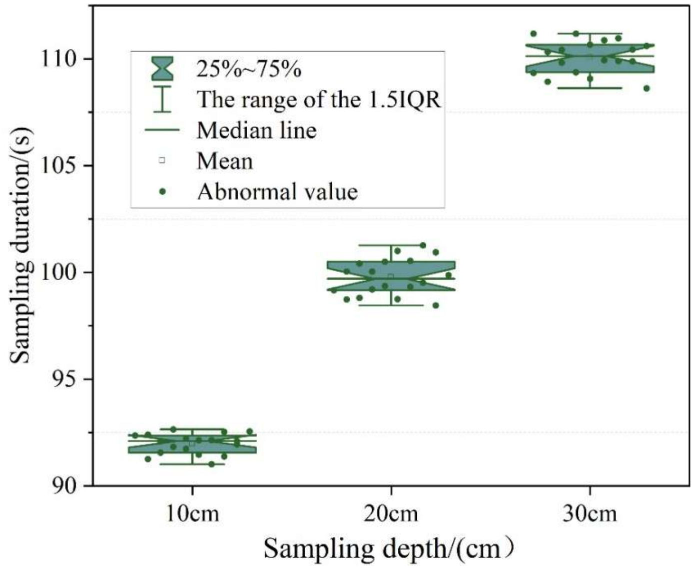

(a) Sampling length and sampling depth

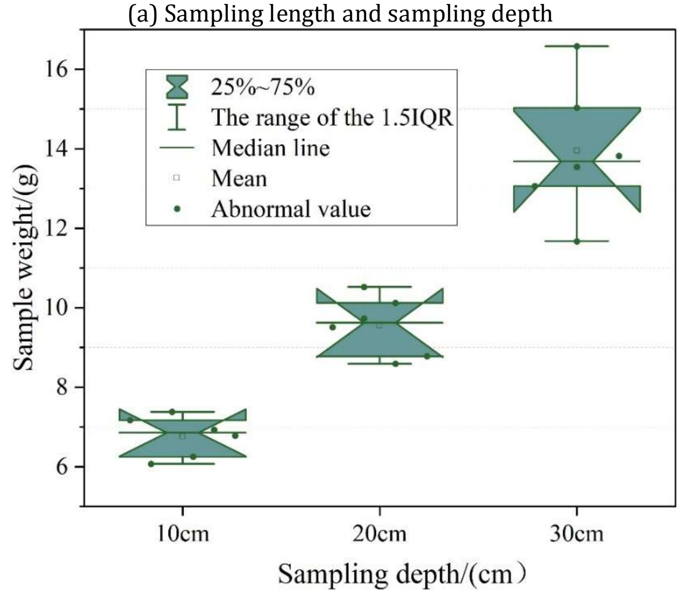

(b) Sample weight and sampling depth

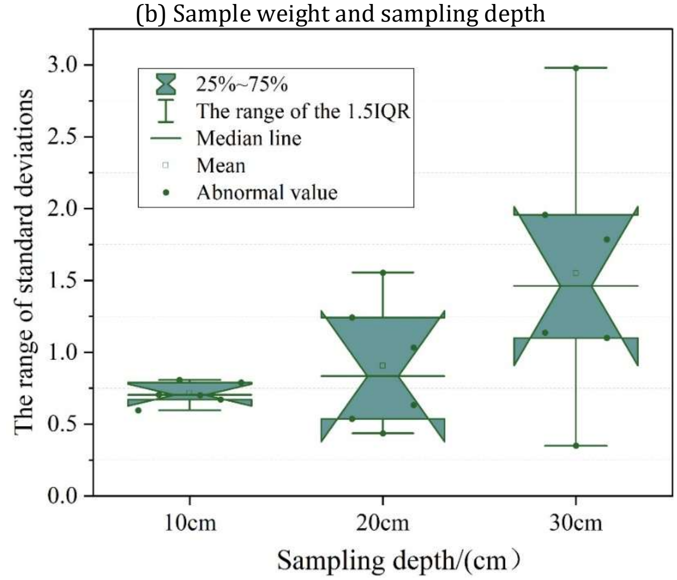

(c) Standard deviation and sampling depth

Fig. 5. The sampling length, the average of the fluid weight and the standard deviation

4.3. *Field sampling of subsurface fluids*

In order to verify the reliability of the fuzzy adaptive design based subsurface fluid sampling device, scientific validity. In this paper, three ways will be used to obtain underground fluids at the sampling sites.

The first sampling method adopts the traditional sampling method, in which the sampling staff goes to the sampling location to obtain the fluid samples from each sampling point using the vertical underground fluid sampler.

The second sampling method uses a UAV-based vertical subsurface fluid sampling system. The sampling point coordinates are preset by the sampling personnel, and the drone hovers over the sampling point in sequence, and the vertical underground fluid sampling device is lowered under the control of the ground station to obtain the fluid samples from each sampling point.

The third type of sampling is based on the fuzzy adaptive design of underground fluid sampling device system.

The manpower and total time consumed by the three sampling methods were 6, 3 and 2 persons, 4 h, 3.2 h and 2.8 h. The UAV-based subsurface fluid sampling system effectively reduces both the manpower consumption and time spent compared with manual sampling. And only need to operate on the shore, personnel do not need to enter the sampling site, to protect the safety of sampling personnel.

Temperature and dissolved oxygen need to be measured on-site due to the rapid change of their physical and chemical properties, so the monitoring indicators are temperature (℃) and dissolved oxygen (mg/L). Dissolved oxygen is a key indicator of biological activity and was measured in this paper based on the possibility of bias due to photosynthesis during transportation of the UAV sampling system.

In order to observe the effects of the three sampling methods in the acquisition of water samples at specified depths, the effectiveness of the fuzzy adaptive design-based subsurface fluid sampling device system designed in this paper was investigated based on the measured values of the middle vertical line of four sections at sampling depths of 1m, 2m, 3m, 4m, and 5m. In order to reduce the chance, the temperature and dissolved oxygen are analyzed in this paper.

According to the sampling scheme, the temperature and dissolved oxygen of manual sampling were measured using a portable dissolved oxygen meter and thermometer, and the UAV-based subsurface fluid sampling system was measured at the shore. Temperature and dissolved oxygen are susceptible to changes in physical and chemical properties in samples transported by UAV. The changes in temperature data at different depths of the middle plumb line under the three sampling methods are shown in Table 2.

Observing the temperature data of underground fluids at different sampling depths, it can be found that there is not much difference in the temperature data obtained by the three sampling methods. Taking the 1-2 sampling plumbline as an example, the temperature data of the three sampling methods are 11.23℃, 11.52℃, and 12.87℃, respectively, with the maximum difference of 1.64℃. In order to meet the underground fluid sampling work that requires high temperature accuracy, the temperature sensor can be added to directly obtain the temperature value of the sampling point in situ.

Table 2. Different depth temperature data changes/(℃)

The middle perpendicular in different sampling modes	Sampling mode	Sampling depth				
		1m	2m	3m	4m	5m
1-2 Sampling perpendicular	1	11.23	10.52	10.56	10.92	11.01
	2	11.52	10.91	11.52	10.05	11.34
	3	12.87	11.04	11.74	11.25	11.57
2-2 Sampling perpendicular	1	11.25	10.93	11.45	11.31	11.52
	2	11.58	11.19	11.36	10.89	11.38
	3	11.76	10.89	11.47	11.34	11.34
3-2 Sampling perpendicular	1	11.21	10.81	10.97	11.23	10.75
	2	11.57	10.95	11.25	10.78	10.64
	3	11.45	10.91	11.26	11.27	11.22
4-2 Sampling perpendicular	1	10.63	10.34	10.78	10.45	10.13
	2	10.76	10.31	10.47	10.45	10.29
	3	10.79	10.15	10.65	10.45	10.29

The variation of DO data at different depths of the intermediate plumb line under the three sampling methods is shown in Table 3. Comprehensive 1-2 sampling plumb line, 2-2 sampling plumb line, 3-2 sampling plumb line, 4-2 sampling plumb line under the three sampling methods of DO data, can be found that manual sampling, vertical sampling, fuzzy adaptive device sampling in the same sampling point of the content of the dissolved oxygen deviation is less and the trend of the changes in different depths is consistent. The mean values of dissolved oxygen at sampling depths of 1m, 2m, 3m, 4m, and 5m for the three sampling methods under the 1-2 sampling plumb line were 7.98mg/L, 7.86mg/L, 8.25mg/L, 7.83mg/L, and 7.77mg/L, respectively. It shows that the use of fuzzy adaptive stratified sampling device has little effect on the index of dissolved oxygen. Therefore, the fuzzy adaptive stratified sampling device system designed in this paper can be applied to the sampling of subsurface fluid indicators with dissolved oxygen as the detection target.

Table 3. Different depth dissolved oxygen data changes/(mg/L)

The middle perpendicular in different sampling modes	Sampling mode	Sampling depth				
		1m	2m	3m	4m	5m
1-2 Sampling perpendicular	1	8.02	7.84	8.23	7.86	7.79
	2	7.87	7.89	8.25	7.81	7.75
	3	8.06	7.86	8.27	7.83	7.77
2-2 Sampling perpendicular	1	7.73	7.85	8.34	8.34	7.89
	2	7.71	7.82	8.29	8.32	7.86
	3	7.76	7.83	8.35	8.29	7.82
3-2 Sampling perpendicular	1	7.42	7.25	7.96	7.55	7.48
	2	7.38	7.29	7.91	7.46	7.46
	3	7.49	7.23	7.93	7.57	7.52
4-2 Sampling perpendicular	1	7.53	7.63	7.48	7.32	7.35
	2	7.60	7.65	7.43	7.41	7.30
	3	7.56	7.64	7.45	7.41	7.40

5. Conclusion

In this paper, by utilizing fuzzy identification algorithm to identify the control system of stratified sampling device, we add the robust adaptive controller of the system model of stratified sampling device, which constitutes the robust adaptive control algorithm of stratified sampling device. Tests are carried out to verify the reasonableness of the stratified sampling device designed in this paper.

When the stratified sampling device system uses a nonlinear control unit to control the system, its output effect is always in a stable state from the initial stage to the end stage. Moreover, the system switching state is obvious, and the switching sequence is based on the control inputs of the nonlinear adaptive controller designed by the fuzzy identification algorithm. The stratified sampling device system assisted by the fuzzy identification method has higher control performance and identification speed.

The sampling depths of 10cm, 20cm and 30cm were used as the sampling depths, and the sampling times of the stratified sampling device system controlled by the fuzzy recognition algorithm were 92s, 100s and 110s, respectively, and the average weights of the underground fluids obtained were 6.76g, 9.54g and 13.95g, and the weights of the samples were also increased with the increase of the sampling depths. The sampling time of each sample is in accordance with the theoretical time, and the system operates stably.

Funding

The Spark Project of Hebei Provincial Seismological Bureau “Research on the Seismic Mechanism of Huanghua Water Level on Stress Field Changes in the Bohai Rim Region Based on Flow Field Characteristics and Coulomb Stress” and “Double difference tomography imaging of crustal structure in the central region of the North China Craton” Joint funding.

References

[1] Zafar, M. W., Saeed, A., Zaidi, S. A. H., & Waheed, A. (2021). The linkages among natural resources, renewable energy consumption, and environmental quality: A path toward sustainable development. Sustainable Development, 29(2), 353-362.

[2] Abiye, T., Masindi, K., Mengistu, H., & Demlie, M. (2018). Understanding the groundwater-level fluctuations for better management of groundwater resource: A case in the Johannesburg region. Groundwater for Sustainable Development, 7, 1-7.

[3] Xiao, W., Zhang, W., Ye, Y., Lv, X., & Yang, W. (2020). Is underground coal mining causing land degradation and significantly damaging ecosystems in semi‐arid areas? A study from an Ecological Capital perspective. Land degradation & development, 31(15), 1969-1989.

[4] Sun, H., Hu, Z., Wang, S., & Song, D. (2024). Long-term effects of underground mining on surface soil moisture and vegetation environment: evidence from the Xishan mining area. Environmental Monitoring and Assessment, 196(12), 1-16.

[5] Hu, Y., Cheng, H., & Tao, S. (2023). Environmental and human health impacts of geothermal exploitation in China and mitigation strategies. Critical Reviews in Environmental Science and Technology, 53(11), 1173-1196.

[6] Du Plessis, A., & du Plessis, A. (2019). Current and future water scarcity and stress. Water as an inescapable risk: current global water availability, quality and risks with a specific focus on South Africa, 13-25.

[7] Jia, X., O'Connor, D., Hou, D., Jin, Y., Li, G., Zheng, C., ... & Luo, J. (2019). Groundwater depletion and contamination: Spatial distribution of groundwater resources sustainability in China. Science of the Total Environment, 672, 551-562.

[8] Huifeng, Y., Wengeng, C., Chuanshun, Z., Zeyan, L., Xilin, B., Yu, R., ... & Yabin, W. (2021). Evolution of groundwater level in the North China Plain in the past 40 years and suggestions on its overexploitation treatment. Geology in China, 48(4), 1142-1155.

[9] Chen, W., Wu, C., Pan, S., & Shi, L. (2024). Analysis on the spatiotemporal evolutions of groundwater hydrochemistry and water quality caused by over-extraction and seawater intrusion in eastern coastal China. Frontiers in Earth Science, 12, 1391235.

[10] Fan, B., Shi, X., Luo, G., Hellwich, O., Ma, X., Shang, M., ... & Ochege, F. U. (2025). Ground subsidence and disaster risk induced by groundwater overexploitation: A comprehensive assessment from arid oasis regions. International Journal of Disaster Risk Reduction, 119, 105328.

[11] Perumal, M., Sekar, S., & Carvalho, P. C. (2024). Global investigations of seawater intrusion (SWI) in coastal groundwaters in the last two decades (2000–2020): a bibliometric analysis. Sustainability, 16(3), 1266.

[12] Li, S., Liu, F., Li, W., Li, C., Huang, F., Jin, S., ... & Ma, X. (2024). Prioritization of organic contaminants in China's groundwater based on national-scale monitoring data and their persistence, bioaccumulation, and toxicity. Science of The Total Environment, 929, 172656.

[13] Sheng, Y., Jiang, W., & Zhang, M. (2023). Mobilization, Speciation, and Transformation of Organic and Inorganic Contaminants in Soil–Groundwater Ecosystems. Applied Sciences, 13(20), 11454.

[14] Zhou, Q., Zhang, J., Xing, K., Wei, J., & Yao, Y. (2024). Groundwater nitrate contamination in China: Spatial distribution, temporal trend, and driver analysis. Environmental Research, 262, 119932.

[15] Zhao, B., Huang, F., Zhang, C., Huang, G., Xue, Q., & Liu, F. (2020). Pollution characteristics of aromatic hydrocarbons in the groundwater of China. Journal of Contaminant Hydrology, 233, 103676.

[16] He, Z., Han, D., Song, X., & Yang, S. (2020). Impact of human activities on coastal groundwater pollution in the Yang-Dai River plain, northern China. Environmental Science and Pollution Research, 27, 37592-37613.

[17] Azzellino, A., Colombo, L., Lombi, S., Marchesi, V., Piana, A., Andrea, M., & Alberti, L. (2019). Groundwater diffuse pollution in functional urban areas: The need to define anthropogenic diffuse pollution background levels. Science of the Total Environment, 656, 1207-1222.

[18] Trefry, M. G., Lester, D. R., Metcalfe, G., & Wu, J. (2019). Temporal fluctuations and poroelasticity can generate chaotic advection in natural groundwater systems. Water Resources Research, 55(4), 3347-3374.

[19] Zeng, B., Zhang, Z., & Yang, M. (2018). Risk assessment of groundwater with multi-source pollution by a long-term monitoring programme for a large mining area. International Biodeterioration & Biodegradation, 128, 100-108.

[20] Kontos, Y. N., Kassandros, T., Perifanos, K., Karampasis, M., Katsifarakis, K. L., & Karatzas, K. (2022). Machine learning for groundwater pollution source identification and monitoring network optimization. Neural Computing and Applications, 34(22), 19515-19545.

[21] Kieft, T. L. (2017). Sampling the subsurface. Hydrocarbon and Lipid Microbiology Protocols: Field Studies, 45-64.

[22] Byrne, D. J., Broadley, M. W., Halldórsson, S. A., Ranta, E., Ricci, A., Tyne, R. L., ... & Barry, P. H. (2021). The use of noble gas isotopes to trace subsurface boiling temperatures in Icelandic geothermal systems. Earth and Planetary Science Letters, 560, 116805.

[23] Houben, G. J., Koeniger, P., Schloemer, S., Gröger-Trampe, J., & Sültenfuß, J. (2018). Comparison of depth-specific groundwater sampling methods and their influence on hydrochemistry, isotopy and dissolved gases–Experiences from the Fuhrberger Feld, Germany. Journal of Hydrology, 557, 182-196.

[24] Formel, N., Enochs, I. C., Sinigalliano, C., Anderson, S. R., & Thompson, L. R. (2021). Subsurface automated samplers for eDNA (SASe) for biological monitoring and research. HardwareX, 10, e00239.

[25] Jianguo, X., Qinghai, Y., Peng, Y., Ze, H., Weite, J., Tao, F. U., & Qingfeng, Y. U. E. (2022). Modular zonal fluid sampling and pressure testing technology for production well. Petroleum Exploration and Development,

49(2), 438-447.

[26] Ueno, A., Tamazawa, S., Tamamura, S., Aramaki, N., Alam Badrul, A. K. M., Murakami, T., ... & Kaneko, K. (2019). Improvement of terrestrial groundwater sampling method affects microbial community analysis. Geomicrobiology Journal, 36(4), 303-316.

[27] Hsieh, P. S., Lin, C. K., Chang, Y. T., Lu, H. Y., & Yang, T. F. (2021). The GTFSampler: A new downhole equipment for geothermal fluid sampling and its testing results in the Chingshiu geothermal field, Ilan, Taiwan. Geothermics, 94, 102077.

[28] Junliang Wu,Wenbin Deng,Fucai Huang,Xiangyang Song,Lin Li & Zhicai Zhai. (2025). Development of a UAV-assisted autonomous water sampling device. Discover Applied Sciences,7(3),182-182.

[29] Chenyang Duan,Ling Yuan,Shijie Zhan,Jian Wang,Jun Dai,Zhengan Tian & Huixian Wu. (2025). Comparison between ballast water sampling skid and traditional ballast water sampling devices: A case study of ship sampling. Marine Pollution Bulletin,210,117284-117284.

[30] Jin Su Oh,Na Yeong Kim,JoonHyeong Park,Hyeonju Jung & Gi Beum Kim. (2024). Nationwide monitoring of freely dissolved polycyclic aromatic hydrocarbons (PAHs) using high speed rotation-type passive sampling device in Korean coastal waters. Marine Pollution Bulletin,209(PB),117175-117175.

[31] Wang Liping. (2024). Fuzzy control system design for landscape lamp of environment art based on multi-function. Proceedings of the Institution of Civil Engineers - Smart Infrastructure and Construction,1-30.

[32] Hicham Khebbache,Naamane Bounar,Yassine Soukkou,Salim Labiod & Abdesselem Boulkroune. (2024). Adaptive estimator-based exponential fault-tolerant tracking control for a class of uncertain MIMO nonlinear systems with simultaneous actuator/sensor faults. Journal of the Franklin Institute,361(17),107202-107202.